

A genetic algorithm used for the intensity level discretization in MLC leaf sequencing for step and shoot IMRT

CHEN Bingzhou^{1,2} ZHANG Conghua² TANG Zhiquan³ HOU Qing^{2,*}

¹ School of Physics Science and Technology, Sichuan University, Chengdu 610064, China

² Key Laboratory of Radiation Physics and Technology, Ministry of Education, Institute of Nuclear Science and Technology, Sichuan University, Chengdu 610064, China

³ Department of Radiation Oncology, Huaxi Hospital, Sichuan University, Chengdu 610041, China

Abstract The inverse planning for a step-and-shoot plan in intensity-modulated radiotherapy (IMRT) is usually a multiple step process. Before being converted into the MLC segments, the optimum intensity profiles of beams, which are generated by an optimization algorithm, shall be discretized into a few intensity levels. The discretization process of the optimum intensity profiles can induce deviations in the final dose distribution from the original optimum dose distribution. This paper describes a genetic algorithm for the discretization of given optimum intensity profiles. The algorithm minimizes an objective function written in terms of the intensity levels. Both the dose-based objective function, which is defined by the deviation between the dose distributions before and after the discretization, and the intensity-based objective function, which is defined by the deviation between the optimum intensity profiles and the discretization intensity profiles, have been adopted. To evaluate this algorithm, a series of simulation calculations had been carried out using the present algorithm, the even-spaced discretization and the *k*-means clustering algorithm respectively. By comparing the resultant discretization-induced deviations (DIDs) in intensity profiles and in dose distributions, we have found that the genetic algorithm induced less DIDs in comparison with that induced in the even-spaced discretization or the *k*-means clustering algorithm. Additionally, it has been found that the DIDs created in the genetic algorithm correlate with the complexity of the intensity profiles that is measured by the “fluence map complexity”.

Key words IMRT, Inverse planning, Step-and-shoot, Discretization

CLC numbers R817.5, O571.33

1 Introduction

Beamlet based inverse planning is one approach commonly used to generate static multileaf collimator (SMLC) plan in IMRT. The inverse planning is usually a multiple step process^[1-3]. First, the optimum intensity profiles that would conduce to a dose distribution best satisfying the given prescription are created by an optimization algorithm. Then, each of the optimum intensity profiles, in which the intensities of the beamlets are continuously variable, is

discretized to form a discrete intensity profile in which the intensity of a beamlet takes a value among a few values that are called the intensity levels. Finally, the discrete intensity profiles are converted into a set of MLC segments by a leaf-sequencing algorithm. In the multiple step process, there are many physical or numerical factors affecting the final quality of the inverse planning. There have been instances in which the inverse planning resulted in unfavorable plans in comparison with that generated by the forward planning^[4]. Thus, identifying the influences of each

Supported by the National Natural Science Foundation of China (Grant No. 10275045) and the Excellent Young Teachers Program of China.

* Corresponding author. E-mail address: bridgezbc@163.com, qhou@263.net

Received date: 2006-05-28

factor and improving the corresponding algorithms are desirable. In this paper, we focus on the study of the discretizing procedure mentioned above.

The simplest discretization algorithm is the even-spaced discretization algorithm that divides the optimum intensity profile into a few evenly spaced intensity levels^[1,2]. This method has the advantage that the generated discrete intensity profile can be sequenced by leaf-sequencing algorithms that create MLC segments of multiple unit weights^[5-7]. However, the final solution would significantly deviate from the original optimization solution, especially when the number of the intensity levels is small^[8]. The deviation could be reduced by using more intensity levels but with the price of dramatic increase in MLC segment number^[5-7].

A method, in which the gradient-based optimization and the discretization of the intensity profile proceeded in turn for a number of iteration steps, were adopted by Keller-Reichenbecher *et al.*^[9] in an attempt to integrate the discretizing procedure with the optimization procedure of the intensity profile. However, the method did not show good convergence behavior and thus the authors actually used only the results obtained by one optimization-discretization step. Recently, Sun *et al.*^[8] applied the simulating annealing algorithm to directly optimize the discrete intensity profile. This method was computationally inefficient. In addition, due to its stochastic nature, the simulated annealing algorithm usually generates intensity profiles of less smoothness^[10].

An alternative approach to reduce the deviation induced in the discretizing procedure is to discrete the optimum intensity profile using unevenly spaced intensity levels, as described by a few groups of authors^[11-13]. The k -means clustering algorithm was applied by Wu *et al.*^[13]. In the k -means clustering algorithm, the initial clusters of the intensities were created in terms of the values of the intensities and a given error tolerance. The deviation between the discrete intensity profile and the optimum intensity profile was diminished by iteratively switching the intensities in adjacent clusters. The k -means clustering algorithm is a local searching algorithm and thus the resultant intensity levels could be potentially suboptimal. The effects of the user defined error

tolerance, equivalently the number of intensity levels, in the k -means clustering algorithm were also studied by Nioutsikou *et al.*^[14].

The discrete intensity profiles of uneven-spaced intensity levels can be sequenced by leaf-sequencing algorithms proposed by Bortfeld *et al.*^[11] and Chen *et al.*^[15]. Thus, the present paper is focused on describing a discretizing method in which an objective function written in terms of the intensity levels is minimized by the genetic algorithm. Using a series of simulated optimum intensity profiles and a clinical case, we have evaluated the algorithm by comparing the discretization-induced deviations (DIDs) in the present algorithm with that in the even-spaced discretization algorithm and the k -means clustering algorithm. It will be shown that our algorithm can result in less DID in the discretization procedure while without losing computational efficiency.

2 Methods

2.1 The objective functions

We have used the *intensity-based objective function* and the *dose-based objective function* to describe the discretization-induced deviations. Assuming that I_i is the intensity of the beamlet i in an optimum intensity profile and the optimum intensity profile is to be discretized into L intensity levels, the intensity-based objective function is defined as

$$O_1(g) = \frac{1}{N_1} \sum_{i=1}^{N_1} [I_i(g) - I_i]^2 \quad (1)$$

where $I_i(g)$ is the intensity of the beamlet i after the discretization and N_1 the number of beamlets in the optimum intensity profile, and

$$g = \{g_0, g_1, \dots, g_L\}$$

With g in an ascending order, denote a number of intensity values to be optimized. As schematically shown in Fig.1, g divides the optimum intensity profile into L groups according to intensity value. The average value of the intensities in the k -th group is written as

$$\varphi_k(g) = \frac{\sum_{i=1}^{N_1} \theta(I_i - g_{k-1}) \theta(g_k - I_i) I_i}{\sum_{i=1}^{N_1} \theta(I_i - g_{k-1}) \theta(g_k - I_i)} \quad \text{for } k = 1, 2, \dots, L \quad (2)$$

which defines the k -th intensity level. The $I_i(g)$ is thus written as

$$I_i(g) = \sum_{k=1}^L \theta(I_i - g_{k-1}) \theta(g_k - I_i) \varphi_k(g) \quad (3)$$

where $\theta(x)$ denotes the step function defined as $\theta(x)=1$, for $x>0$ and otherwise $\theta(x)=0$.

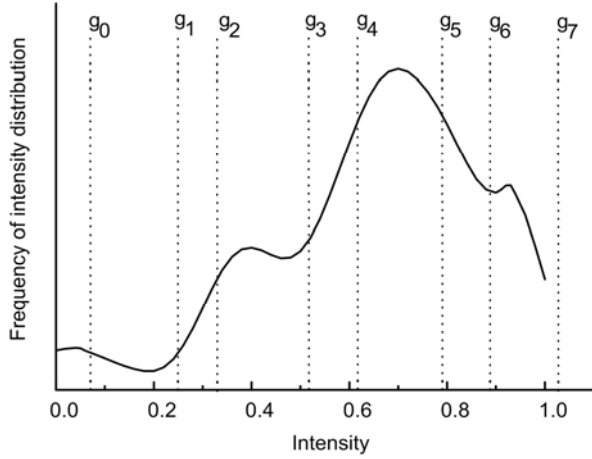


Fig.1 A schematic graph explaining the present algorithm. For a given optimum intensity profile, the intensity histogram are divided into a few sections by a set of values g_i ($i=0,1,\dots,L$) where L is the preset number of the intensity levels. The intensity levels to be created are the average of the beamlet intensities in each section. The algorithm searches the optimal values of g_i that make the given objective function minimal.

Because induced deviation in dose distribution is ultimately concerned in the discretization process, we also used the *dose-based objective function* $O_D(g)$ that is defined by the deviation between the dose distributions before and after the discretization is to be minimized. $O_D(g)$ is thus written

$$O_D(g) = \frac{1}{N_v} \sum_n \left(\sum_i I_i(g) d_n^{(i)} - \sum_i I_i d_n^{(i)} \right)^2 \quad (4)$$

where $d_n^{(i)}$ is the dose on voxel n contributed by i -th beamlet of unit weight, and N_v the number of voxels involved. $I_i(g)$ is also determined by Eqs. (2) and (3). Note the objective function $O_D(g)$ is not equivalent to $O_I(g)$. To demonstrate this, let us consider a schematic example in which we have only one intensity level φ and thus $I=\varphi$ for all the beamlets. $O_I(g)$ is thus written

$$O_I(g) \equiv O_I(\varphi) = \sum_{i=1}^{N_i} (\varphi - I_i)^2$$

Then, $O_I(\varphi)$ is minimized at

$$\varphi = \frac{1}{N_I} \sum_{i=1}^{N_I} I_i$$

where

$$\frac{\partial O_I(\varphi)}{\partial \varphi} = 0$$

However, the gradient of the *dose-based objective function*

$$\frac{\partial O_D(\varphi)}{\partial \varphi}$$

is not zero at

$$\varphi = \frac{1}{N_I} \sum_{i=1}^{N_I} I_i$$

In principle, using the *dose-based objective function* should induce least deviation in terms of dose distribution, however, it is more computer time consuming. Thus, the results obtained by using the *dose-based objective function* can be used for evaluating intensity-based discretization approaches.

2.2 The genetic algorithm

We used the genetic algorithm to minimize the objective function $O_I(g)$ and $O_D(g)$. This algorithm was designed to be independent of the concrete form of the objective functions. To construct the chromosomes in the genetic algorithm, we introduced the scaled intensity values

$$\bar{g} = \{ \bar{g}_0, \bar{g}_1, \dots, \bar{g}_L \}$$

with

$$0 \leq \bar{g}_i \leq 1$$

Assuming the maxima intensity of a given optimum intensity is I_{\max} , the scaled intensity values are defined by

$$g = \alpha I_{\max} \bar{g} \quad (5)$$

where α is a parameter larger than unit. The resultant g are thus in a range from 0 to αI_{\max} . A chromosome is thus encoded by the decimal digits of \bar{g} . For example, in case $L=5$ and the user defined digital precision $N_D=3$, a chromosome encoded by

$$\bar{g} = \{0.01, 0.345, 0.528, 0.715, 0.823, 0.946\}$$

is (01034528715823946). In practices, $N_D=5$ was used.

A generation contains N_P chromosomes $\bar{g}^{(j)}$ for $j=1, 2, \dots, N_P$ with j denoting the j -th chromosome. Each of them results in the objective value $O(g^{(j)})$. We generated the initial generation by assigning $\bar{g}^{(j)}$ with random values from 0 to 1. Then a generation evolves to next generation following the operations of selection, crossover, mutation and replacement. The process is similar to that described in detailed in a previous paper of ours for beam orientation optimization in IMRT^[16]. The process can be outlined as follows.

(a) The chromosomes in current generation are ranked according to their objective value $O(g^{(j)})$;

(b) Two chromosomes are selected by the roulette wheel selection. The probability for a chromosome to be selected is determined by its rank;

(c) The crossover between the selected chromosomes is performed at a randomly selected cut-point with the probability p_c . Two offspring are generated;

(d) The offspring undergo mutation at a randomly selected point with probability p_m ;

(e) Step (b)-(d) are repeated for n_r times to generate $2n_r$ offspring to replace the chromosomes that are last ranked in the current generation. A new generation is thus created. The chromosomes in the new generation are decoded and the objective function $O(g^{(j)})$ are calculated;

f) Step (a)-(e) are repeated and the process stops at the generation J_m where the convergence criteria or the preset maximum generation is reached. The final solution is denoted by

$$I \equiv I(g^{(J_m)}) = \{I_1(g^{(J_m)}), I_2(g^{(J_m)}), \dots, I_{N_I}(g^{(J_m)})\}$$

By experiments, the parameters N_P , p_c and p_m were selected as 100, 0.5 and 0.025 respectively to guarantee the process converges.

2.3 Evaluation method of the algorithm

For a discretization intensity profile I , we used the standard deviation in intensity profile S_I , the standard deviation in dose distribution S_D and the γ index^[17] to measure the deviation induced in discretizing the optimum intensity profile. The standard deviation in intensity profile S_I and the standard deviation in dose distribution S_D are defined

respectively

$$S_I = \frac{1}{N_I} \sum_i (I_i - \bar{I}_i)^2 \quad (6)$$

and

$$S_D = \frac{1}{N_v} \sum_n (\sum_i I_i d_n^{(i)} - \sum_i I_i \bar{d}_n^{(i)})^2 \quad (7)$$

Note S_I and S_D share the similar forms of the objective functions $O_I(g)$ and $O_D(g)$, however, I_i here refer to the final discretization intensity profile obtained by a discretization algorithm.

The γ index was firstly introduced by Low *et al* to quantitatively compare calculated dose distributions and measured dose distributions. Here, we regard the dose distribution $d_{opt}(r)$ created by the optimum intensity profile as the standard for the comparison. In the γ index methodology, the vector $\{r, d_{opt}(r)\}$ defines a point in 4-dimensional position-dose space. Assuming the dose distribution created by the discrete intensity profile is $d_{dis}(r')$, $\{r', d_{dis}(r')\}$ forms a track in the position-dose space when r' is run in the whole position space. The γ index at position r is thus defined as the closest scaled-distance between point $\{r, d_{opt}(r)\}$ and the track $\{r', d_{dis}(r')\}$, that reads

$$\gamma(r) = \min \{ \Gamma(r, r') \} \forall \{r'\} \quad (8)$$

where $\Gamma(r, r')$ is the scaled-distance

$$\Gamma(r, r') = \sqrt{\frac{R^2(r, r')}{\Delta_R^2} + \frac{D^2(r, r')}{\Delta_D^2}} \quad (9)$$

With

$$R = |r' - r|$$

and

$$D(r, r') = d_{dis}(r') - d_{opt}(r)$$

the standard value Δ_R was chosen to be 3 mm and Δ_D 0.03. As far as dose distributions are concerned here and also in S_D , we used a modified version of superposition-convolution algorithm^[18,19], which can produce the dose matrix of beamlets. The voxel size in the dose calculations was chosen as 2mm×2mm×2mm. This size could be too coarse to calculate the γ index at r . Thus, we divided the voxels around r into fine voxels of size of 0.2mm×0.2mm×0.2mm and the dose distribution $d_{dis}(r')$ in these fine voxels was calculated using linear interpolation of the doses on the 2mm×2mm×2mm voxels. The distribution function $\gamma(r)$

probe the difference between dose distributions at given positions. It is convenient to introduce the γ index histogram $P(x)$ that is defined as the percentage of positions in test that have $\gamma \geq x$. The positions included in the calculations of the γ index are only those at which at least one of the dose distributions $d_{\text{opt}}(r)$ and $d_{\text{dis}}(r)$ is nonzero.

To compare the present algorithm with other algorithms, we have implemented the even-spaced discretization algorithm and the k -means clustering algorithm. The implementation of the k -means clustering algorithm followed that described in detail in literatures^[13], other than no constraints on the difference between adjacent intensity levels was imposed.

3 Results

The aim of this paper is to present a general algorithm used for discretizing a given optimum intensity profile in IMRT. Thus, we used simulated optimum intensity profiles as well as a clinical case to test the algorithm.

3.1 The simulated case

The testing phantom used for dose calculations was of cubic geometry and was discretized into $2\text{mm} \times 2\text{mm} \times 2\text{mm}$ voxels. The field sizes were $10\text{cm} \times 10\text{cm}$ and $5\text{cm} \times 5\text{cm}$. For each of the field sizes, the beamlet size were $1\text{cm} \times 1\text{cm}$ and $0.5\text{cm} \times 0.5\text{cm}$ respectively. The ‘optimum’ intensity profiles used for the testing were created by randomly assigning the beamlet intensities with values ranging from Φ_{min} to Φ_{max} . In this study, we choose $\Phi_{\text{max}}=1$ and $\Phi_{\text{min}}=0.2$, $\Phi_{\text{min}}=0.4$, $\Phi_{\text{min}}=0.6$ and $\Phi_{\text{min}}=0.8$ respectively. For each combination of Φ_{min} , the field sizes and beamlet sizes, we created 10 test intensity profiles. Varying the parameters Φ_{min} results in profiles of different complexity that could be, in some degree, quantified by the ‘‘fluence map complexity’’ (FMC), that is defined as the standard deviation of the adjacent beamlet intensities in leaf travel direction^[20]. For a two-dimensional intensity profile, the FMC is written as

$$\text{FMC} = \frac{1}{N_b} \sum_{r=1}^{N_y} \sqrt{\sum_i (I_i^{(r)} - 0.5I_{i-1}^{(r)} - 0.5I_{i+1}^{(r)})^2}$$

where i is the index of beamlet in leaf travel direction and N_y is the number of rows of beamlets in the perpendicular direction. N_b is the total number of beamlets. A small Φ_{min} usually leads to larger fluctuations in the intensity profiles and thus larger FMC values.

With these test intensity profiles, we carried out intensity profile discretizations using the number of intensity levels $L=5, 7$ and 10 . For the convenience of narration, we designate the genetic algorithm using the *intensity-based objective function* as IBGA, the genetic algorithm using the *dose-based objective function* as DBGA, the even-spaced discretization algorithm as ESA and the k -means clustering algorithm as KMA. The results generated by these algorithms are denoted by corresponding superscripts.

Fig.2a shows the comparison of S_I data obtained by using IBGA, DBGA, ESA and KMA for the cases that the field size was $10\text{cm} \times 10\text{cm}$ and the beamlet size $1\text{cm} \times 1\text{cm}$. The three panes, from left to right, correspond to the number of intensity levels $L=5, 7$ and 10 respectively. From left to right in each pane, the data points correspond to descending complexities of the test intensity profiles, i.e., $\Phi_{\text{min}}=0.2, 0.4, 0.6$ and 0.8 respectively. Each of the data points is the average value of S_I obtained from ten test intensity profiles. Generally, the IBGA results in the lowest S_I . Since minimization of the DID in intensity profile is in accordance with the optimization goal of IBGA, $S_I^{(\text{IBGA})}$ is lower than $S_I^{(\text{DBGA})}$, however, the difference is small. $S_I^{(\text{IBGA})}$ and $S_I^{(\text{DBGA})}$ tend to be coincident when the number of intensity levels is large, or the intensity profile is less complex. $S_I^{(\text{KMA})}$ is obvious higher than $S_I^{(\text{IBGA})}$ and $S_I^{(\text{DBGA})}$. At large L and Φ_{min} , the difference between $S_I^{(\text{KMA})}$ and $S_I^{(\text{IBGA})}$ and $S_I^{(\text{DBGA})}$ diminishes, however, the difference between $S_I^{(\text{ESA})}$ and $S_I^{(\text{IBGA})}$ and $S_I^{(\text{DBGA})}$ is more significant. Fig.2b shows the corresponding S_D data. Since the DBGA directly minimize the DID in dose distribution, the DBGA results in the lowest S_D . The difference between $S_D^{(\text{DBGA})}$ and $S_D^{(\text{IBGA})}$ is minimal and diminishes as L becomes large and the intensity profiles become complex. It is evident that DBGA and IBGA result in less DID in dose distribution in comparison with that result by the ESA and the KMA.

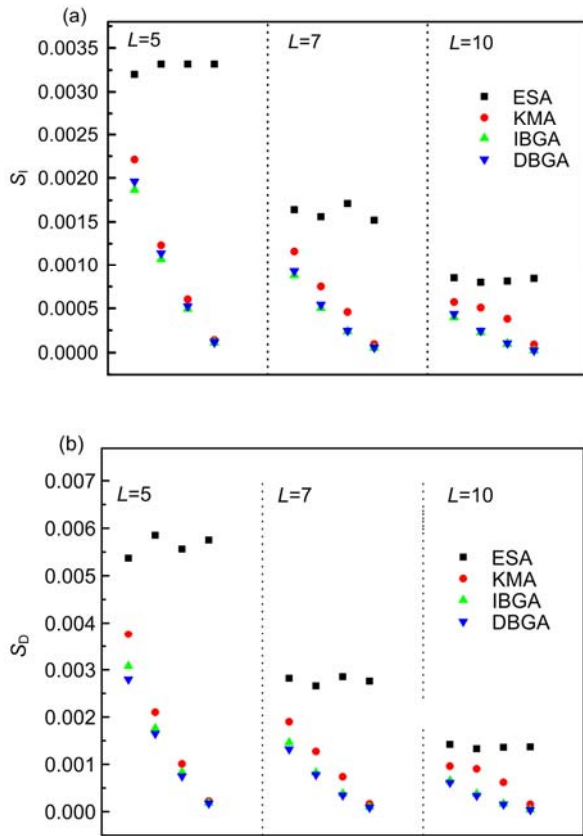


Fig.2 The standard deviation in intensity profile S_I (a) and in dose distribution S_D (b) obtained by IBGA, DBGA, KMA and ESA for the field size 10cm×10cm and the beamlet size 1cm×1cm.

It is also observed in Fig.2 that, on average, S_I or S_D of the IBGA and the DBGA descend monotonically with the decrease of the complexity of the intensity profiles that was navigated by Φ_{min} . Corresponding to the second pane in Fig.2, Fig.3 displays in detail the relationships between the FMC and S_I as well as S_D for all the test intensity profiles of field size 10cm×10cm at $L=7$. It is observed that the data points of the IBGA and the DBGA are least scattered in comparison with the data points of the KMA, while the ESA data points are too scattered to show any correlation between the DID and FMC. The correlation between the DID and the complexity of the intensity profiles could be of interests in the consideration that, when a smoothing filter is applied in the intensity profile optimization that creates the optimum intensity profiles, the correlation makes the effect of the smoothing on the DID more anticipatable. Similar conclusion could be drawn by the results obtained by using different field size and the beamlet size.

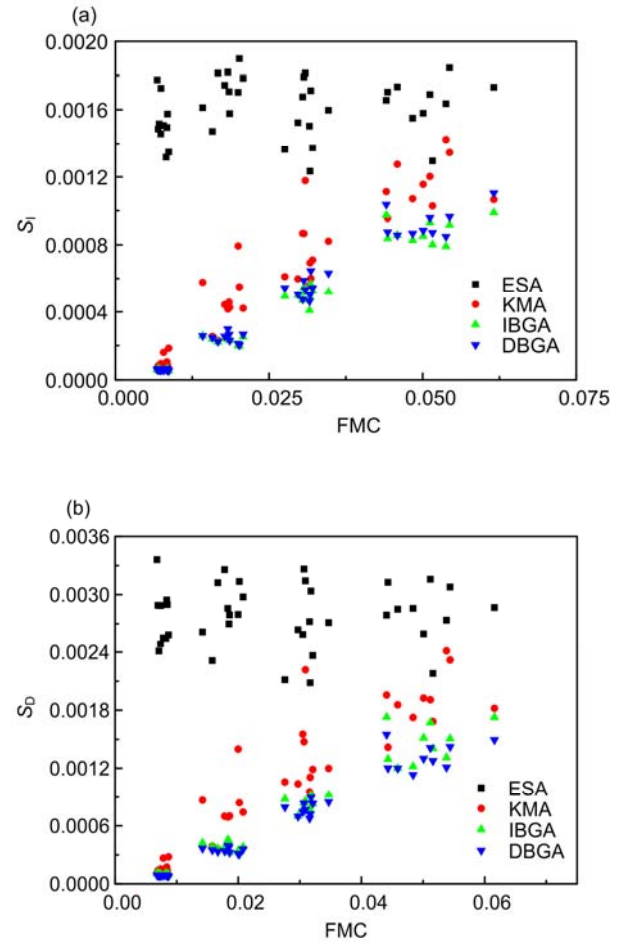


Fig.3 The relationship of S_I (a) and S_D (b) with the fluence map complexity (FMC) of the test intensity profiles. The results were obtained by IBGA, DBGA, KMA and ESA for the field size 10cm×10cm, the beamlet size 1cm×1cm and the number of intensity level $L=7$.

Fig.4 shows the γ index histograms $P(x)$ for the number of intensity levels $L=7$. Each of the histograms was also the average over ten histograms obtained by ten test intensity profiles with field size 10cm×10cm and beamlet size 1cm×1cm. Φ_{min} used to generate the test intensity profiles was 0.2 and the corresponding FMC on average is 0.0505. Generally, the γ index histograms of the IBGA and the DBGA are very close and hardly to be distinguished. Both $P^{(IBGA)}(x)$ and $P^{(DBGA)}(x)$ are obviously lower than $P^{(KMA)}(x)$ and $P^{(ESA)}(x)$.

For example, at $x=0.5$, $P^{(IBGA)}$, $P^{(DBGA)}$, $P^{(KMA)}$ and $P^{(ESA)}$ are 2.8%, 3%, 4.2% and 6.5% respectively. Results for alternative FMC values also display the similar feature.

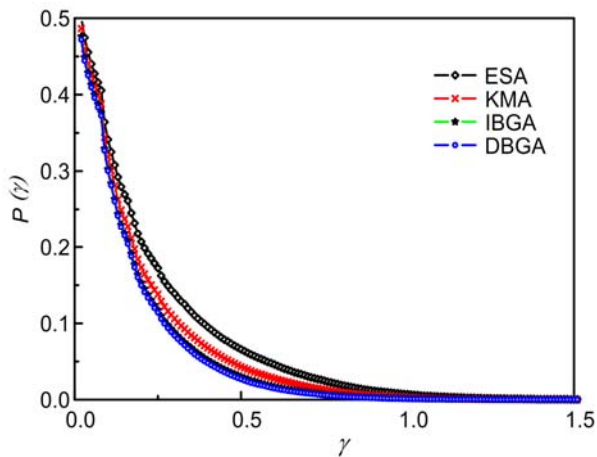


Fig.4 The histogram of the γ index obtained by IBGA, DBGA, KMA and ESA using the number of intensity levels $L=7$. The field size was $10\text{cm}\times 10\text{cm}$, and the beamlet size was $1\text{cm}\times 1\text{cm}$. Each curve was the average of ten histograms obtained by ten test intensity profiles of $\Phi_{\min}=0.2$. The average FMC of the intensity profiles is 0.0505.

3.2 The clinical case

The clinical case used for testing was a complicated case for IMRT treatment of the tonsil. This case had been used in a previous paper of ours^[21]. In this case, there were three PTVs that were prescribed to doses of 66, 60, and 54 Gy, respectively. The dose-volume constraint for the left parotid was no more than 20% of the volume could be overdosed above 15 Gy. The constraint for the right parotid was no more than 60% of the volume could be overdosed above 25 Gy. Hard constraints were imposed to the spinal cord, brain stem, and sub-mandibular gland with the dose limits of 45, 50 and 25 Gy, respectively. Fig.5 shows an axial slice of the patient anatomy. The voxel size of this phantom is $2\text{mm}\times 2\text{mm}\times 2\text{mm}$.

The clinical case was planned using five evenly spaced 6 MV photon beams. The optimum intensity profiles were created by the simulated dynamics algorithm^[22]. In this process, the beamlet sizes of $1\text{cm}\times 1\text{cm}$ and $0.5\text{cm}\times 0.5\text{cm}$ were used respectively. The discretizations of the optimum intensity profiles were carried out by IBGA with the number of intensity levels $L=5, 7$ and 10 respectively. For comparison, ESA and KMA were also used for discretizing the optimum intensity profiles. Because similar conclusions can be drawn from data generated by using different beamlet sizes, only the results obtained by using beamlet size $1\text{cm}\times 1\text{cm}$ are shown.

Fig.6a shows the comparison of S_I data obtained

by using IBGA, ESA and KMA. For all beams and all values of L , the IBGA induces the least S_I and the ESA induces the largest S_I . For $L=5$, the differences between $S_I^{(\text{IBGA})}$ and $S_I^{(\text{KMA})}$ as well as $S_I^{(\text{ESA})}$ are obvious. For $L=7$, $S_I^{(\text{IBGA})}$ and $S_I^{(\text{KMA})}$ in the second beam and the fifth beam tend to be close, but $S_I^{(\text{IBGA})}$ and $S_I^{(\text{KMA})}$ remain different in the other beams. For $L=10$, the difference between $S_I^{(\text{IBGA})}$ and $S_I^{(\text{KMA})}$ diminishes. Fig.6b shows the corresponding S_D data. It is evident that the IBGA result in the least S_D in comparison with those of ESA and KMA.

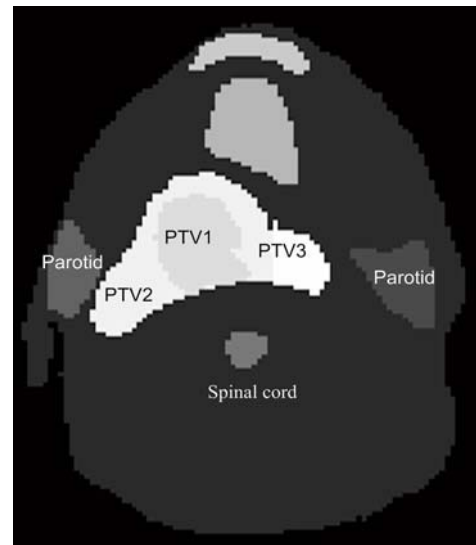


Fig.5 An axial slice of the clinical case used for testing the discretization algorithm.

Fig.7 shows the γ index histograms $P(x)$ for the number of intensity levels $L=7$. It is observed that $P^{(\text{IBGA})}$ is lower than $P^{(\text{KMA})}$ and $P^{(\text{ESA})}$ for all γ values. The percentage of dose points of $\gamma\geq 1$ is about 4%, 6% and 8% for IBGA, KMA and ESA respectively.

The DID can be also demonstrated by DVHs. Fig.8 compares the DVHs generated by the original optimum intensity profile and the discretization intensity profiles of IBGA, KMA and ESA with the number of intensity levels $L=7$. It is observed that the discretization induced degradation in the DVHs of the PTVs, while the degradation in the DVH of the parotids is minor. Generally, the degradation induced by IBGA is the least. Especially for the PTV1, the DVH generated by IBGA is significantly better than the DVHs generated by KMA and ESA. This result suggests again that the present algorithm for discretizing optimum intensity profiles created less DIDs.

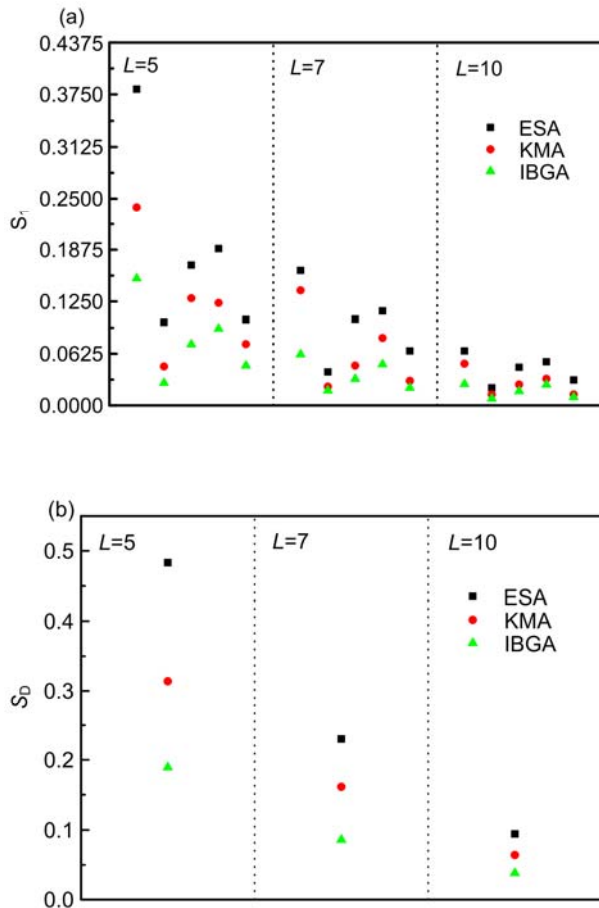


Fig.6 The standard deviation in intensity profile S_1 and in dose distribution S_D for the clinical case. Five evenly spaced beams were used and the optimum intensity profiles of the beams were generated by the simulated dynamics algorithm. The first pane displays the standard deviation for the number of intensity levels $L=5$, the second pane for $L=7$ and the third pane for $L=10$ separately. (a) S_1 for each beam; (b) S_D for the total dose distribution.

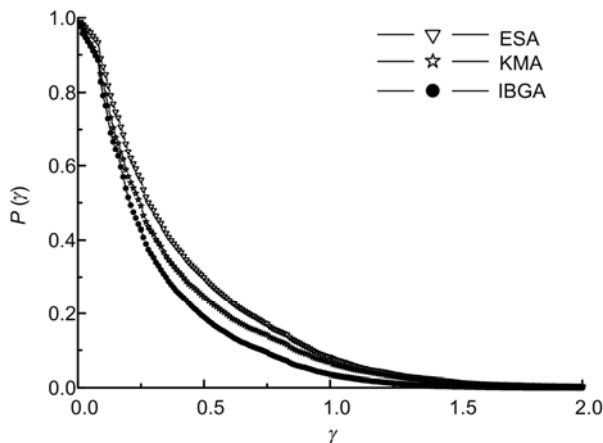


Fig.7 The comparison of the histograms of the γ index obtained by IBGA, KMA and ESA using the number of intensity levels $L=7$ for the clinical case.

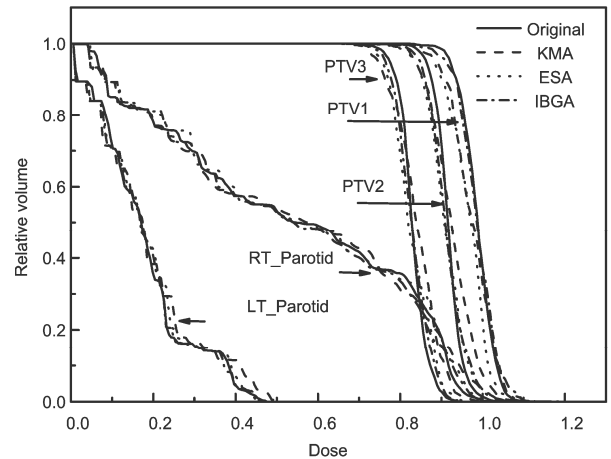


Fig.8. The comparison of the DVHs created by the original optimum intensity profiles and the discretization intensity profiles of the IBGA, KMA and ESA that used the number of intensity levels $L=7$ for the clinical case.

A question that may be concerned is if the IBGA will induce much more MLC segments to achieve the improvement in dose distribution. For a given discretization intensity profile, the number of segments may depend on the segmentation algorithm and a specific delivery mode. In this paper, the segmentation algorithm by Bortfeld for step-and-shoot mode was implemented^[1]. Table 1 shows the number of segments for the clinical case for intensity levels $L=5, 7$ and 10 . Generally, the IBGA results in more segments, however, the increase of the segment number is minor in respect to the improvement in dose.

Table 1 Comparison of the number of segments under different clustering algorithms and different numbers of intensity levels for the clinical case

Beamlet size: 1cm×1cm			
	ESA	KMA	IBGA
$L=5$	33	35	36
$L=7$	48	48	50
$L=10$	67	66	72

4 Discussion and conclusion

An issue that is often concerned with in the inverse planning for IMRT is how optimal the final solution could be achieved. Even under a well-defined objective function, the final solution could deviate from the real optimal solution, due to the physical and

numerical approximations in the inverse planning. A number of authors have investigated this issue from different perspectives. For example, based on the commonly used dose-based objective function with dose-volume constraints, Llacer *et al*^[20] and Wu and Mohan^[23] had investigated the effects of multiple local minima in the intensity profile optimization. Their numerical results indicated that the multiple local minima did not pose a clinically significant problem. That conclusion had been confirmed by the theoretical analysis of Alber *et al*^[24]. Thus, the afterward procedures have likely more marked effects.

In the present paper, we have put the focus on another source of numerical error, i.e., the deviation induced in discretizing the intensity profiles obtained in the previous optimization procedure. We have described the genetic algorithm used for the intensity profile discretization. Both the *intensity-based objective function* and the *dose-based objective function* have been used. In principle, the genetic algorithm using the *dose-based objective function* induces the least DID in dose distribution and thus, in spite of its low computational efficiency due to a lot of dose calculation involved, can be used as a tool to evaluate the IBGA and other discretization algorithms. Our testing results have shown that the differences between the DIDs created by the IBGA and the DBGA are small. We therefore recommend the IBGA for routine uses because its computational efficiency is much higher than that of the DBGA. On a PC with a Pentium IV 2.6 GHz processor, the IBGA takes about 1s of CPU time for a field of 100 beamlets and the total time is linearly proportional to the total number of beamlets of all the fields. In the calculations, the genetic algorithm evolved for 500 generations. Actually, the convergence had been reached at about 200 evolution generations. The IBGA and the DBGA are global searching algorithms. The comparison between the IBGA and the KMA has show the advantage, in terms of the DID in both the intensity profiles and the dose distributions, of the IBGA over the KMA. The advantage of the IBGA over the ESA is more prominent, especially when the number of intensity levels is small and the intensity profiles are complex.

In the interest of improving the delivery

efficiency in SMLC, a number of authors have addressed the smoothing of optimization intensity profiles^[21,25,26]. One can expect that the DID could also be reduced by smoothing the optimum intensity profiles. In the present study, it has been observed that the correlation between the DID and the complexity, which was measured by the FMC, depend on the discretization algorithms. Stronger correlation between the DID in IBGA and FMC has been observed than the correlation in KMA and ESA. This feature of the IBGA should make the smoothing of the optimum intensity profiles more benefiting in the reduction of the DID.

Acknowledgments

We would like to thank Dr. Chen Yan for supplying the clinical example used in this paper.

References

- 1 Bortfeld T R, Kahler D L, Waldron T J, *et al.* *Oncol Biol Phys*, 1994, **28**: 723–730.
- 2 Chui C S, Chan M F, Yorke E, *et al.* *Med Phys*, 2001, **28**: 2441–2449.
- 3 Webb S. *Intensity-modulated radiation therapy*, IOP Publishing Limited, 2001.
- 4 Vaarkamp J, Adams E J, Warrington A P, *et al.* *Radiother Oncol*, 2004, **73**: 65–72.
- 5 Galvin J, Chen X, Smith R. *Int J Radiat Oncol Biol Phys*, 1993, **27**: 697–705.
- 6 Siochi R A. *Int J Radiat Oncol Biol Phys*, 1999, **43**: 671–680.
- 7 Xia P, Verhey L J. *Med Phys*, 1998, **25**: 1424–1434.
- 8 Sun X, Xia P, Yu N. *Med Phys*, 2004, **31**: 2402–2411.
- 9 Keller R M A, Bortfeld T, Levegrun S, *et al.* *Int J Radiat Oncol Biol Phys*, 1999, **45**: 1315–1324.
- 10 Coolens C, Evans P M, Seco J, *et al.* *Phys Med Biol*, 2004, **9**: 3857–3875.
- 11 Bar W, Alber M, Nusslin F. *Phys Med Biol*, 2001, **46**: 1977–2007.
- 12 Beavis A W, Ganney P S, Whitton V J, *et al.* *Phys Med Biol*, 2001, **46**: 2457–2465.
- 13 Wu Y, Yan D, Sharpe M B, *et al.* *Med Phys*, 2001, **28**: 2188–2197.
- 14 Nioutsikou E, Bedford J L, Christian J A, *et al.* *Med. Phys*, 2004, **31**: 892–901.
- 15 Chen Y, Hou Q, Galvin J M. *Med Phys*, 2004, **31**:

-
- 1504–1511.
- 16 Hou Q, Wang J, Chen Y, *et al.* Med Phys, 2003, **30**: 2360–2367.
- 17 Low D A, Harms W B, Mutic S, *et al.* Med Phys, 1998, **5**: 656–661.
- 18 Boyer A, Mok E. Med Phys, 1985, **12**: 169–177.
- 19 Mackie T R, Scrimger J W, Battista J J. Med Phys, 1985, **12**: 188–196.
- 20 Llacer J, Deasy J O, Bortfeld T R, *et al.* Phys Med Biol, 2003, **48**: 183–210.
- 21 Hou Q, Zhang C H, Wu Z W, *et al.* Med Phys, 2004, **31**: 1339–1347.
- 22 Hou Q, Wang J, Chen Y *et al.* Med Phys, 2003, **30**: 61–68.
- 23 Wu Q, Mohan R. Med Phys, 2002, **29**: 1514–1527.
- 24 Alber M, Meedt G, Nusslin F, *et al.* Med Phys, 2002, **29**: 2584–2589.
- 25 Alber M, Nusslin F. Phys Med Biol, 2000, **45**: N49–N52.
- 26 Spirou S V, Fournier B N, Yang J, *et al.* Med Phys, 2001, **28**: 2105–2112.